NASA-CR-202382

ODERACS 2 White Spheres Optical Calibration Report

Culp, Robert D.[1] Gravseth, Ian[2] Wantuch, Todd[3]
Gloor, Jason [3]

Colorado Center for Astrodynamics Research
Department of Aerospace Engineering Sciences
University of Colorado
Boulder, CO 80309-0431

University Contract No. 1536400

NASA Reseach Grant NAG 9-768

January 9, 1995

[1]Professor and Chairman
[2]NASA Graduate Student Research Fellow
[3]Undergraduate Research Assistant

Contents

List of Tables

List of Figures

Abstract

This report documents the status of the Orbital Debris Radar Calibration Spheres (ODERACS) 2 white spheres optical calibration study. The purpose of this study is to determine the spectral reflectivity and scattering characteristics in the visible wavelength region for the white spheres that were added to the project in the fall, 1994. Laboratory measurements were performed upon these objects and an analysis of the resulting data was conducted.

These measurements are performed by illuminating the objects with a collimated beam of light and measuring the reflected light versus the phase angle. The phase angle is defined as the angle between the light source and the sensor, as viewed from the object. By measuring the reflected signal at the various phase angles, one is able to estimate the reflectance properties of the object.

The methodology used in taking the measurements and reducing the data are presented.

The results of this study will be used to support the calibration of ground-based optical instruments used in support of space debris research. Visible measurements will be made by the GEODDS, NASA and RADOT telescopes.

Chapter 1

Introduction

This report documents the Orbital Debris Radar Calibration Spheres (ODERACS) 2 preflight optical calibration study of the two supplemental white spheres delivered to the University of Colorado in fall, 1994. The paper presents the visible region spectral reflectivity and scattering characteristics for the ODERACS 2 white spheres. The results of this study will be used to support the calibration of ground-based optical instruments in support of space debris detection research.

This report is organized such that the main body contains the essential information and the appendixes are used to present a more detailed analysis. The basic setup, data reduction methods, results, and discussion of the results are presented. More information on the ODERACS project, the test objects, and the tasking can be found in Appendix A.

Chapter 2

Methodology

The setup and procedure for the preflight optical calibration of the spheres were driven by the need to have both scattering and specular measurements sufficient to find the albedo over the visible region from 450 nm to 950 nm wavelengths. The statement of work specified that the measurements were to be taken, to the extent possible, at phase angles from ~0 to ~180 degrees in 5° intervals. The measurements were taken over all possible angles where the sensor did not interfere with or enter the light beam.

Measurements were taken for the two white spheres. A spectrometer capable of performing efficiently this large number of measurements was used. The spectrometer uses a fiber-optic cable to attach the sensor to the processing box. This cable allows the sensor to be moved easily for the many phase angle measurements. Appendix D contains more information about the spectrometer. Figure 2.1 shows the basic setup for the experiment. Appendix B contains more sketches and discussion of the apparatus and setup.

2.1 Procedure

Before the flight hardware was tested, the experimental system was aligned and tested. A rehearsal of the experimental process was conducted to assure correct handling of the flight hardware. Appendix F contains more information on the handling precautions implemented for the experiment.

Once the equipment was ready, the objects were placed in position and measurements were taken over the entire phase angle range in a timely manner. Measurements of the direct light signal were made for use in calculation of the albedo. This process was repeated for each object. After each object was tested, it was returned to its carrying case.

2.2 Light sources

The objects were illuminated with a 1000 Watt Quartz-Halogen light source reflected through a planar secondary mirror and a high precision parabolic mirror to form a highly collimated light beam which closely resembles solar conditions. This high energy light source was needed to provide enough light for the spectrometer to work accurately and efficiently.

The direct signal spectrum for the 1000 W light is shown in Figure 2.2. It can be seen that at extreme wavelengths the direct signal is not very strong. Due to the nature of the

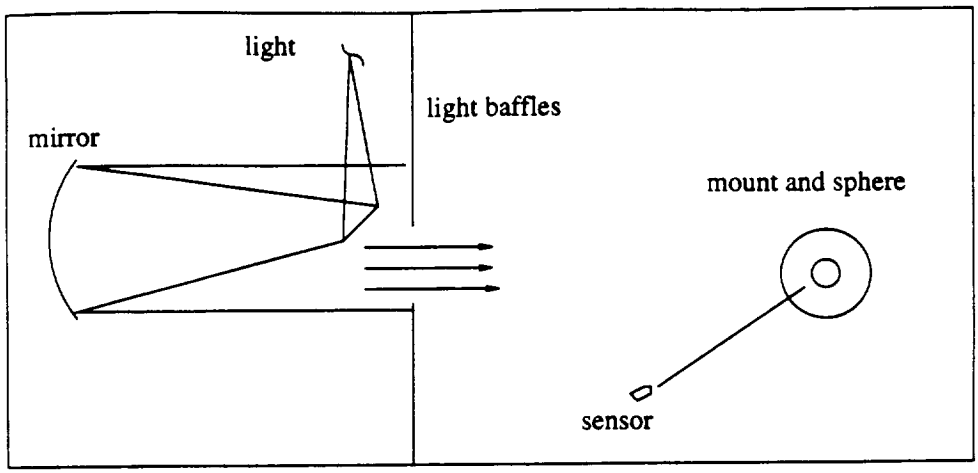

Figure 2.1: Basic experiment setup

light source and the noise of the spectrometer, the data is not reliable below 450 nm or above 950 nm.

2.3 Spectrometer

The spectrometer used in this study is a LabSpec Spectrometer, developed by Analytical Spectral Devices, Inc (ASD) of Boulder, Colorado. The sensor, which feeds the spectrometer, is attached via a fiber-optic cable to the body of the spectrometer. This made it easy to take measurements at various phase angles.

The spectrometer is run by a PC, which drives the spectrometer and stores the data. It was found that the drift in the noise of the spectrometer was noticeable for the longer integration times and weak signals. More information on the spectrometer is found in Appendix D. Information on how the drift was removed from the data is found in Appendix G.

2.4 Phase angle

Measurements at many phase angles were taken so that the albedo and the percentage of light scattered could be estimated. The phase angle θ, as shown in Figure 2.3, is the angle between the line from the test object to the source and the line from the test object to the sensor, as viewed from the object. The measured angle θ and the actual phase angle 2ϕ for the light measured are somewhat different because of the limited range to the sensor. The difference between these two values can be easily calculated from the geometry of the setup, and is discussed in Appendix G.

Multiple phase angle measurements allow the scattering and specular signals to be decoupled and gives one the ability to estimate the total reflected light. This total reflected light is used to obtain the albedo estimate. There are several definitions for albedo, which are described in Appendix G. For this work albedo is:

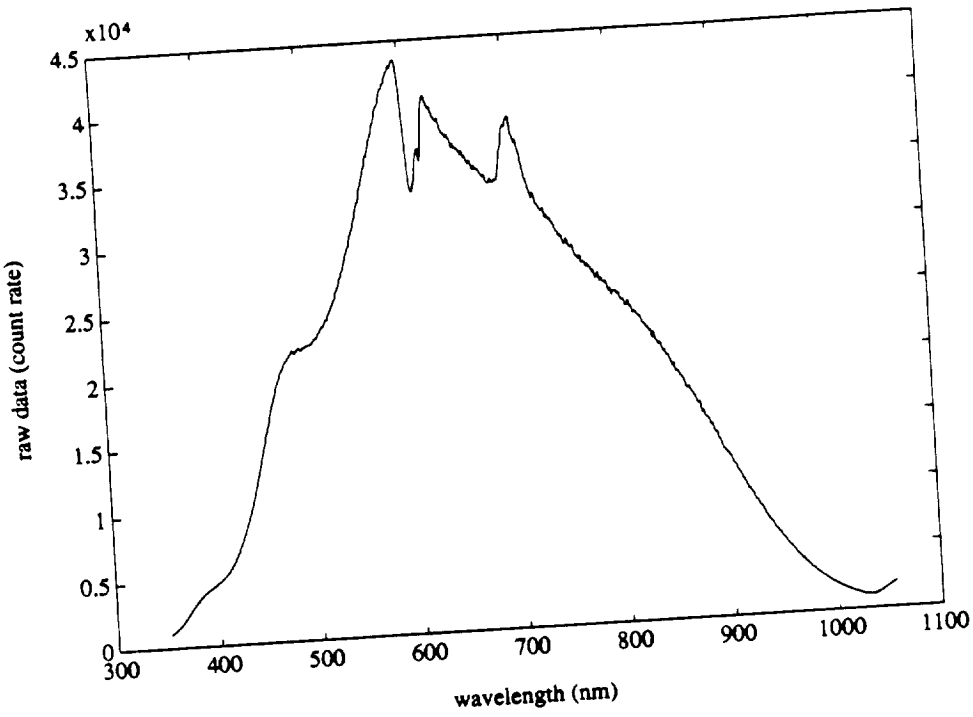

Figure 2.2: Direct light signal vs wavelength

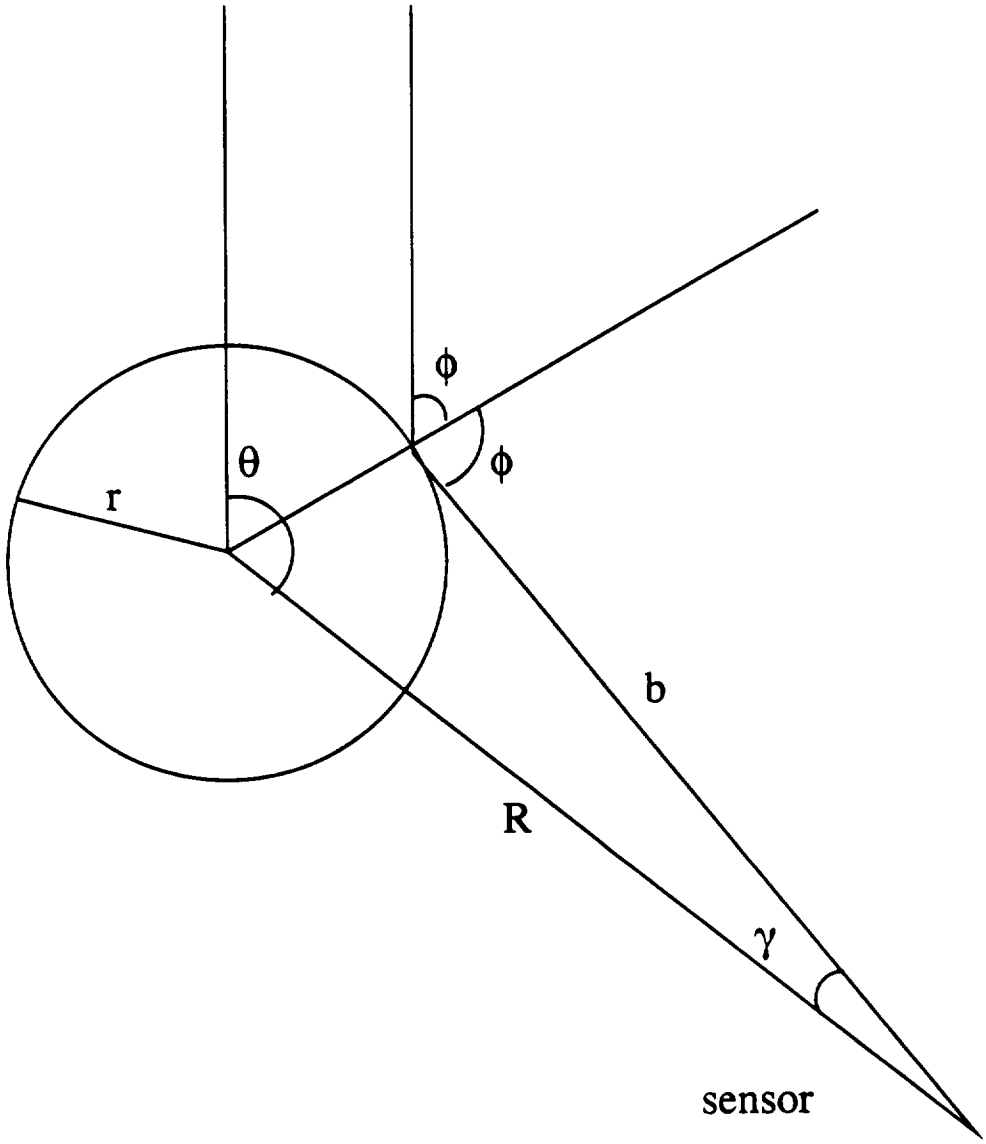

Figure 2.3: Phase angle definition. This is a top view of the sphere-sensor setup (not to scale).

$$\text{Albedo} = \frac{\text{total reflected light}}{\text{total incident light}} \tag{2.1}$$

For a perfect specular reflection, under unobtainable ideal conditions, one would see a constant intensity from evenly collimated light coming off a sphere at all phase angles. For a perfectly diffuse surface, which scatters light as a Lambertian surface, one sees a very distinct falloff in signal with phase angle. Even for the highly polished spheres, the reflection is not perfectly specular. Both specular and scattering characteristics are observed for the white spheres.

The following equations illustrate the two parts of the light signal from a perfectly diffuse and perfectly specular reflection, respectively. These equations represent the ideal diffuse and specular signals viewed at a far distance such that the source can be treated as a point source.[1] This is discussed more in Appendix G. Figure 2.4 shows the idealized diffuse, specular and sum of those two signals for albedo equal to one and with 50 percent of the light scattered diffusely.

$$\text{Diffuse} \qquad E_r = \frac{2aEr^2}{3\pi R^2}[\sin\theta + (\pi - \theta)\cos\theta] \tag{2.2}$$

$$\text{Specular} \qquad E_r = \frac{aEr^2}{4R^2} \tag{2.3}$$

where

$E_r \equiv$ Reflected flux
$E \equiv$ Incident flux
$a \equiv$ Albedo
$r \equiv$ Radius of sphere
$R \equiv$ Range to sensor
$\theta \equiv$ Phase angle

2.5 Data processing

Due to the large number of measurements taken on each object, the data processing was the most difficult portion of this study. Programs were written to immediately analyze the data from the objects to determine if the albedo and scattering results were reasonable. Then at a later time, the data was plotted up and analyzed more carefully.

The above equations for the specular and diffuse signals are idealized equations with the far field approximation. Due to the limitations of the spectrometer and setup, the ratio of R to r was between 5 and 25. For the smaller $\frac{R}{r}$ values the far field approximation is violated. Therefore modified values for the phase angle and range were used in the albedo estimation. This is discussed more in Appendix G.

[1] Personal communication with Dr. John Lambert, Rockwell Int., Colo. Spr., CO

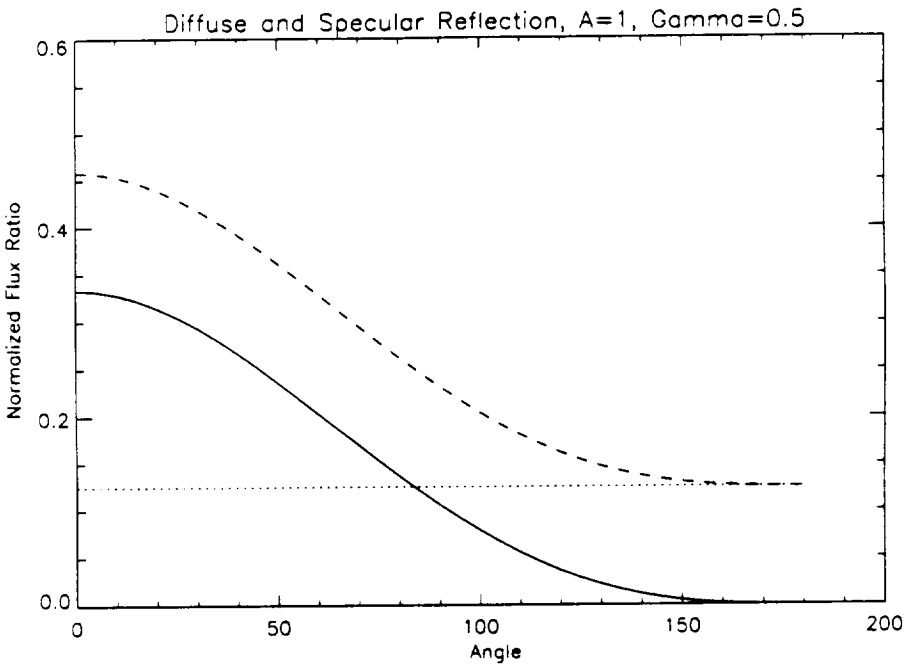

Figure 2.4: Diffuse versus specular signals

Chapter 3

Results and Discussion

This section contains the basic results of the study and a discussion of those results. The albedo-scattering plots along with the best fit and raw data plots for the two white spheres are located in Appendix H.

3.1 Spheres

The reflectance properties were obtained using methods described in Appendix G. The albedo values presented here are the average values of the most reliable tests run for each sphere. The basic equation for the spheres is repeated again below, where the term on the left hand side of the equation is referred to as the normalized signal.

$$\frac{E_r R^2}{E r^2} = \frac{\xi \cdot \gamma \cdot 2a}{3\pi}[\sin\theta + (\pi - \theta)\cos\theta] + (1 - \gamma) \cdot \frac{a}{4} \tag{3.1}$$

$E_r \equiv$ Reflected flux
$E \equiv$ Incident flux
$a \equiv$ Albedo
$r \equiv$ Radius of sphere
$R \equiv$ Range to sensor
$\theta \equiv$ Phase angle
$\gamma \equiv$ Percentage of light scattered
$\xi \equiv$ Proportion of Sphere Viewed (Due to limited sensor range)

The albedo and scattering values for the spheres from this experiment are presented in Tables 3.2. The results for these surfaces appear consistent within themselves and with visual inspection of the surfaces.

The main errors in reducing the data seem to be the drift of the spectrometer and a small range-to-radius ratio. The drift rate problem is discussed in detail in Appendixes D and G, but is outlined here. The spectrometer has a certain background noise which changes with temperature. As the temperature of the room fluctuates the background noise drifts. This is a problem because the drift rate over the cycle of measurements can be of the same

Material	Nature of surface	Coefficient
Aluminum, Polished	Specular	0.69
Steel, Polished	Specular	0.55
Chromium	Specular	0.62
Platinum	Specular	0.62

Table 3.1: CRC values for reflection coefficients

magnitude as the actual measurements. In addition to the drift, there is some random noise in the signal.

Many measurements were made of the drift rate for the spectrometer. This drift rate can be effectively removed for the wavelengths with the stronger signals. Due to the much smaller light strength at the extreme wavelengths, the errors at these wavelengths are expected to be higher.

The low signal-to-noise ratio for the spectrometer under the lighting conditions for this experiment force the sensor to be placed close to the spheres. This in turn created a low range to sensor over radius of sphere ratio, $\frac{R}{r}$. The equations shown for the expected fluxes from the diffuse and specular components were derived for a sensor at a large $\frac{R}{r}$ ratio. These equations are still reasonable approximations for this study, but modifications to these equations are being studied.

A low value for this ratio also meant that the range to the specular reflection point was not constant over the measured phase angles. Correcting for this varying value of the range was performed for the white spheres. The same range correction was used for the white spheres as for the specular reflecting spheres in previous ODERACS tests. The correction is discussed in Appendix G.

Since there is a falloff in signal when the sensor is not pointed directly at the incoming light and the white spheres reflect a portion of light diffusely, the measured signal will be somewhat lower than its true value. This error was not compensated for and will reduce the measured signal an amount depending on the ratio, $\frac{R}{r}$.

Attempts were made to compensate for all the above mentioned errors.

3.1.1 Albedo and scattering

The albedo and scattering values for the white spheres are presented in Table 3.2. These values represent the average and standard deviation for the best measurements on the individual spheres. It should be noted that the estimates for the scattering have much larger errors than the standard deviation indicates.

The albedo values from both estimation methods agree well with each other for the spheres.

The estimates of the scattering for the spheres were very sensitive to small changes in the signal and should be treated with caution. The scattering component of the spheres comes from the off-bore sight directions, which suffer from signal degradation. This will cause the scattering component to be underestimated. Unfortunately, only one method was used to estimate the scattering component for the spheres, so there is not a backup method with which to compare the scattering estimates.

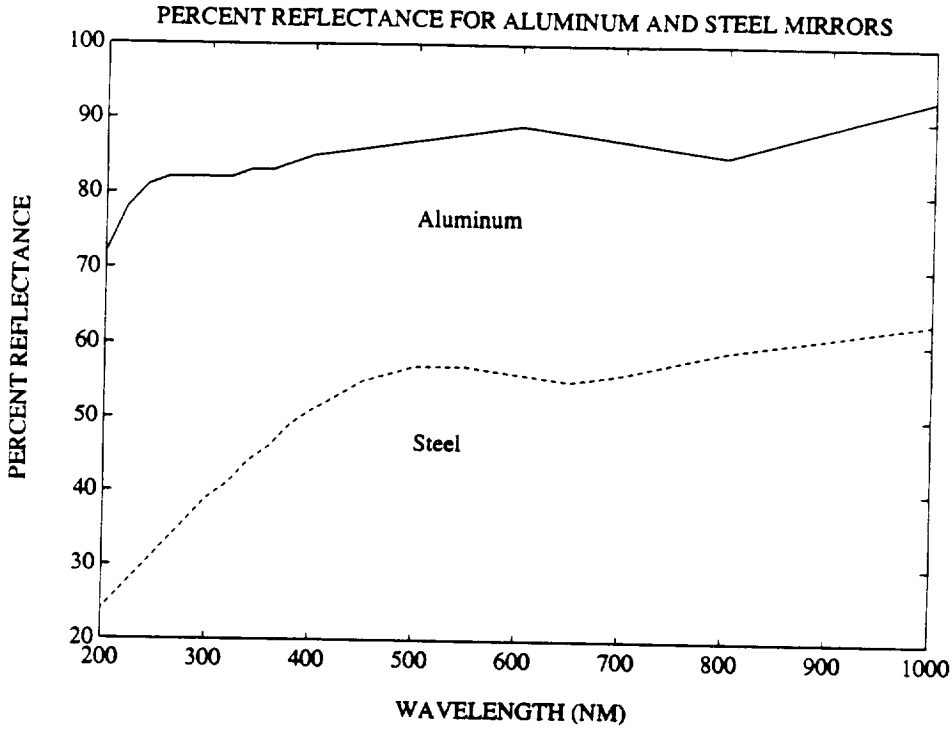

Figure 3.1: Reflectance of metal mirrors from Allen

Sphere ID	Size of Sphere	Type of Sphere	Albedo	Deviation	Scattering	Deviation
SN1008	4	White	.7794	.041	.8168	.014
SN1012	4	White	.7654	.031	.8216	.054

Table 3.2: Scattering and albedo values for white spheres

Chapter 4

Conclusions

The methodology and results for the ODERACS 2 white spheres preflight optical calibration study have been presented. The calculated albedo and gamma coefficients for both white spheres are consistent between tests.

4.1 Acknowledgements

The authors would like to acknowledge two people for their contributions to this study. Dr. William McClintock of the Laboratory for Atmospheric and Space Physics (LASP) for the use of his laboratory, equipment, and time, and also Glen Cress for his role as liaison between CU and JSC.

4.2 References

Allen, C.W. Astrophysical Quantities. Third Ed., The Athlone Press, London, 1973, pg. 108.

CRC Handbook of Chemistry and Physics, 62nd Ed, CRC press, Boca Raton, 1981, pg E-386.

Egan, W.G. and T. Hilgeman. *Applied Optics*, Vol. 15, No. 7, July 1976, pp. 1845-1849.

Egan, W.G. and T. Hilgeman. *Applied Optics*, Vol. 16, No. 11, November 1977, pp. 2861-2864.

Hapke, B. and E. Wells, "Bidirectional Reflectance Spectroscopy I - Theory", *Journal of Geophysical Research*, Vol 86, No B4, April 10, 1981, pp 3039-3054.

Hapke, B. and E. Wells, "Bidirectional Reflectance Spectroscopy II - Experiments and Observations", *Journal of Geophysical Research*, Vol 86, No B4, April 10, 1981, pp 3055-3060.

Lompado, A., B.W. Murray, J.S. Wollam, and J.F. Meroth, "Characterization of optical baffle materials." *SPIE Proceedings Series: Scatter from Optical Components*, Vol. 1165, 1989, pp. 212-226. Proceedings of a conference, 8-10 August, 1989, San Diego, CA.

Madler, R.A., R.D. Culp, and T.D. Maclay. "ODERACS II pre-flight optical calibration." To be presented as the 1993 SPIE Aerospace and Remote Sensing Conference, Orlando, Florida, 12-16 April, 1993, Paper 1951-06.

Marx, E. and T.V. Vorburger. "Light scattered by random surfaces and roughness determination." *SPIE Proceedings Series: Scatter from Optical Components*, Vol. 1165, 1989, pp.72-86. Proceedings of a conference, 8-10 August, 1989, San Diego, CA.

Press, W.H., B.P. Flannery, S.A. Teukolsky, and W.T. Vertterling. Numerical Recipes: The Art of Scientific Computing. Cambridge University Press, Cambridge, 1986.

Rambauske, W.R. and R.R. Gruenzel. *J. Am. Opt. Soc.*, Vol. 55, No. 3, March 1965, pp. 315-318.

Stover, J.C. Optical Scattering: Measurements and Analysis. McGraw-Hill, N.Y., 1990.

Veverka, J. "Photometry of Satellite Surfaces," in Planetary Satellites, ed. Joseph Burns, University of Arizona Press, Tucson, 1977.

Appendix A

ODERACS Project, Spheres and Tasking

A.1 ODERACS project

This report is an important part of the NASA Orbital Debris Radar Calibration Spheres (ODERACS) 2 project. The overall goal of this project is to provide reference targets for the calibration of both radar and optical sensors for small orbital debris objects.

The purpose of this study is to determine the spectral reflectivity and scattering characteristics in the visible wavelength region for various objects. These measurements are used to determine an approximate albedo and phase angle scattering as a function of wavelength for the spheres.

ODERACS is a project of the Solar System Exploration Division at JSC, and is a joint effort between JSC, GSFC, NCSU, DoD, Phillips Lab, the USAF, the University of Colorado, and others.

A.2 Tasking

The statement of work for the preflight optical calibration is summarized below.

A.2.1 Task : Flight Spheres Calibration

Using unpolarized light, the absolute visible spectral reflectivity and scattering characteristics of all flight spheres are to be determined between 4500 and 9500 Angstroms. The data is to be sufficient to obtain albedo, and to generate phase angle scattering plots as a function of wavelength. Spectral measurements are to be made within bands of 800 Angstroms, or less, and at intervals of 500 Angstroms, or less. Scattering measurements are to be made at phase angles from near-zero degrees to near 180 at 5 degree or smaller steps. Plots and tabular listing of the spectral reflectivity as a function of scattering angle are to be prepared for each sphere.

If it may be reasonably assumed that the spheres are uniform, there will be not need to examine more than one portion of the sphere. However, since this is not likely to be the case, the spheres should be measured at five individual orientations.

Appendix B

Experimental Setup

B.1 Experimental Setup

The purpose of this experimental setup was to simulate as closely as possible the solar radiation incident upon an object in orbit about the Earth in order to estimate the reflectance characteristics for several objects. The light that was used had to be collimated (parallel light rays) and controlled to fall only on the object that the spectrometer was measuring. All other light was blocked out by means of baffles, see sketches. The primary light source used was a 1000-watt light bulb with a constant power supply, see Appendix E.

Figure 1 details the basic equipment setup used in this experiment. The sphere mount and parabolic mirror were placed at opposite ends of the table, primarily because of space constraints. The light source was placed at a distance of 90 inches from the center of the parabolic mirror, the focal length. Figure 2 details the 4 inch flat mirror was used to reflect the initial light beam into the parabolic mirror. The distance from the bulb to the flat mirror and from the flat mirror to the parabolic mirror was 13 and 77 inches respectively.

Several measures were taken to absorb or block extraneous light. The experiment was conducted in a black painted room and all light from outside was sealed out. The baffles used were fitted carefully together and covered over the top with black felt, forming a large black box in which the light source was placed. This allowed only a simple beam of light to emerge past the baffles. However, the parabolic mirror was not contained in this enclosed region because it had to be placed some seven feet away at one end of the table. This was the primary source of extraneous light. Another source of unwanted light was from the mount on which the objects were placed. Even though the collimated beam illuminated only the target, secondary reflectance was produced from the light reflected down from the target and onto the mount.

Figure 3 details the sphere mount used in this testing. The mount itself had a built in angular protractor which made angle measurements easy and accurate. The mount stood 11 in. high and was covered with black felt. Additionally, an extended platform (arm) was connected to the side of the mount which was used to attach the spectrometer's sensor.

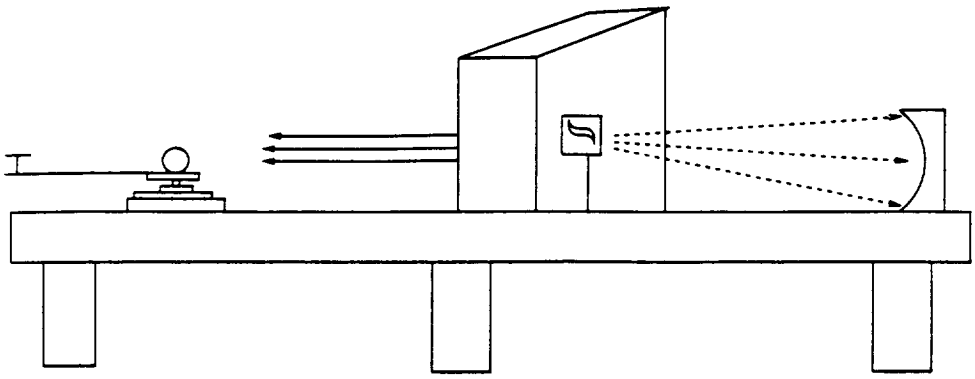

Figure B.1: Basic experiment setup - side view

The spheres were placed onto a ring to prevent them from rolling off the horizontal surface. Figure 4 shows a diagram of the sphere mount. As a result a very small portion of each sphere dipped below the rim of the ring and was hidden from the light beam. It was felt that this was a logical step so that the safety of the spheres could be insured.

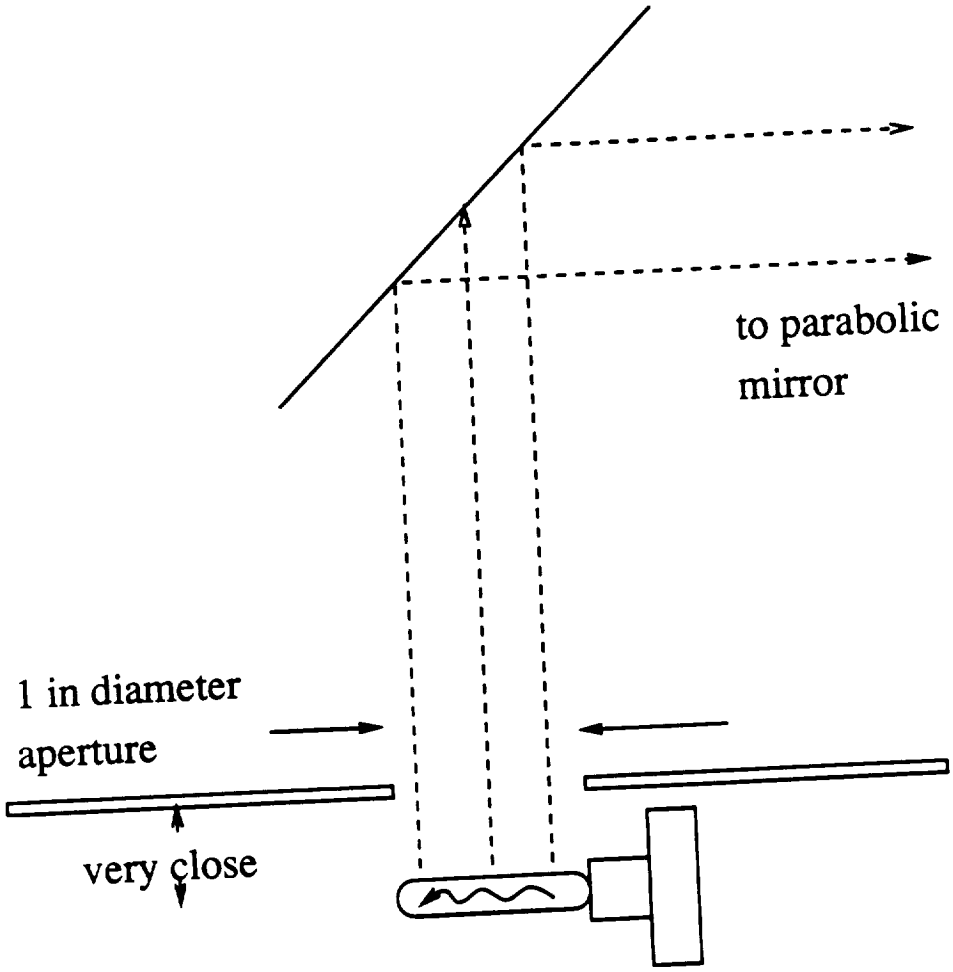

Figure B.2: Main light source configuration

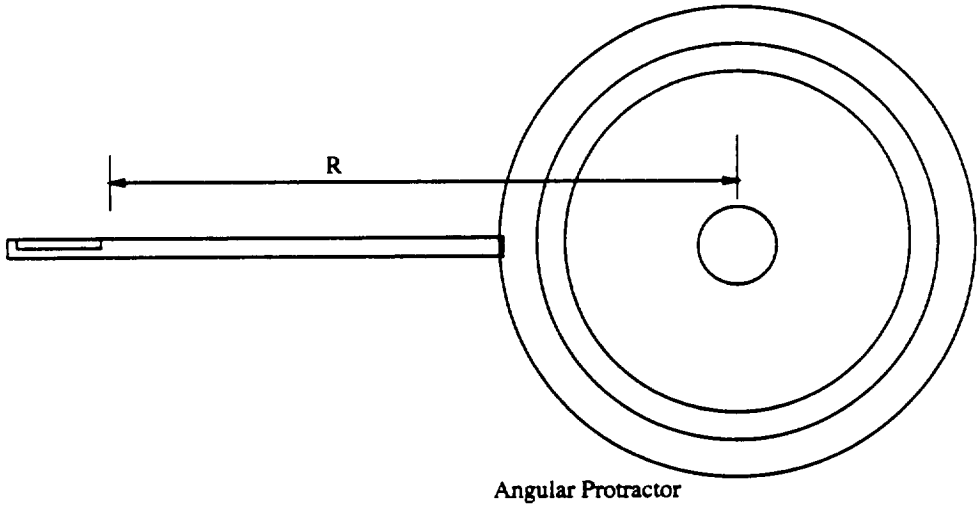

Figure B.3: Sensor mount configuration

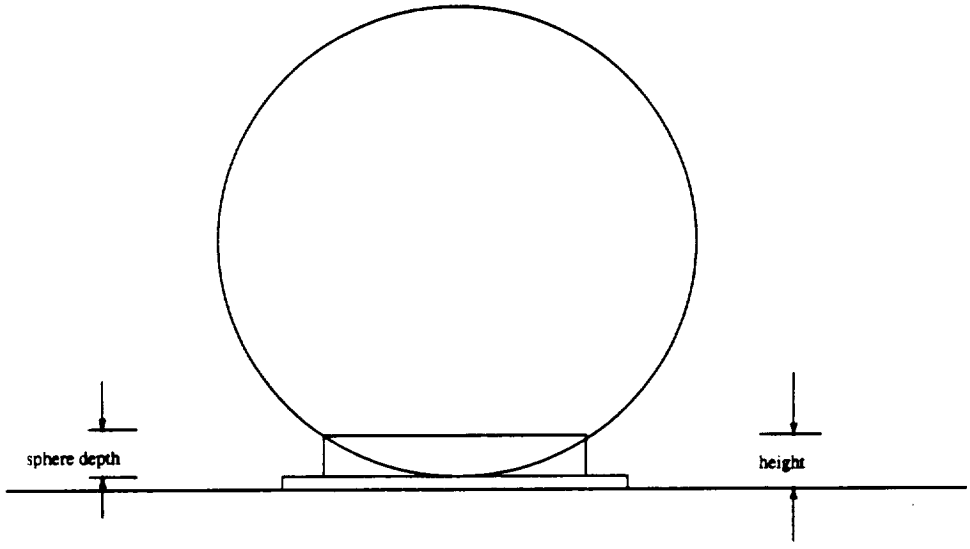

Figure B.4: Sphere mount

Appendix C

Procedure

Each day before testing, the laboratory equipment used in this experiment was set up and aligned. The sphere mount was centered on the test stand and the foam pads were aligned to insure that the test object would not be damaged if it happened to fall off the stand. After all of the lab equipment was set up and properly aligned, the sphere to be tested was removed from its storage compartment. To protect the surface of the sphere, lint-free gloves over talc-free rubber gloves were worn whenever any of the spheres were handled.

After placing the object on its mount and rechecking the set-up, all the lights in the room were extinguished, and an appropriate integration time was chosen for the set of measurements. Measurements were then taken in 5 degree increments, starting as close to zero degrees as was possible without letting the sensor interfere with the light stream. Several dark readings were taken so that the spectrometer's drift could be measured. Typically, measurements were taken until about 165 degrees. The angle of the sensor could be measured accurately down to fractions of a degree. After the object was measured, a measurement of the direct light signal was taken.

When the measurements were completed, the sphere was returned to the carrying case. Then a quick analysis of the data was performed to make sure the data looked reasonable. The data was then transferred to a UNIX platform via a floppy disk for future analysis.

Appendix D

Spectrometer

The spectrometer used for this laboratory experiment was a LabSpec, designed and built by Analytical Spectral Devices, Inc. (ASD) of Boulder. It has 512 channels for data sampling, utilizing a plasma coupled photodiode array, with spectral range of 347.7 to 1056.6 nm. It has integration times ranging from 17 milliseconds up to 9 minutes. The spectrometer's noise can be removed either manually or automatically. The sensor utilizes fiber optics, and it has a two meter cable so that the sensor can be easily moved. The sensor itself consists of a fiber optics bundle that is roughly .6 mm in diameter at its terminus.

Although on the whole the spectrometer was well suited for this experiment, it also had a significant amount of drift in its dark signal over time, partially due to temperature fluctuations within the room. While this drift would be relatively insignificant for measurements being taken under sunlight, with this laboratory experiment the amount of noise in the signal was significant, especially when viewing the test article with long integration times and small reflected signals.

Since the signal had a significant drift in it, the drift was subtracted from the signal by assuming that the drift between two successive dark measurements was approximately linear. This provides an acceptable estimation of the signal for the wavelengths with a strong signal, but causes the extreme wavelength calculations to be unreliable. For this reason the extreme wavelengths have not been used in the calculations.

This spectrometer comes with a laser pointing device so that the sensor is easily pointed at the specular point. The laser pointing device is necessary to correctly align the bore sight of the sensor. This is necessary due to the signal falloff at angles offset from the bore sight. This signal falloff as a function of off-axis angle is shown in Figure D.1. For the specular spheres analyzed in previous experiments this does not introduce significant errors due to the specular nature of these objects. However, for the more diffuse objects a significant signal comes from the off-bore sight directions. For this reason, these objects were viewed from as great a range as possible to reduce the maximum off-axis angle. Nevertheless, the estimated albedos of the diffuse objects are most likely underestimated in this experiment.

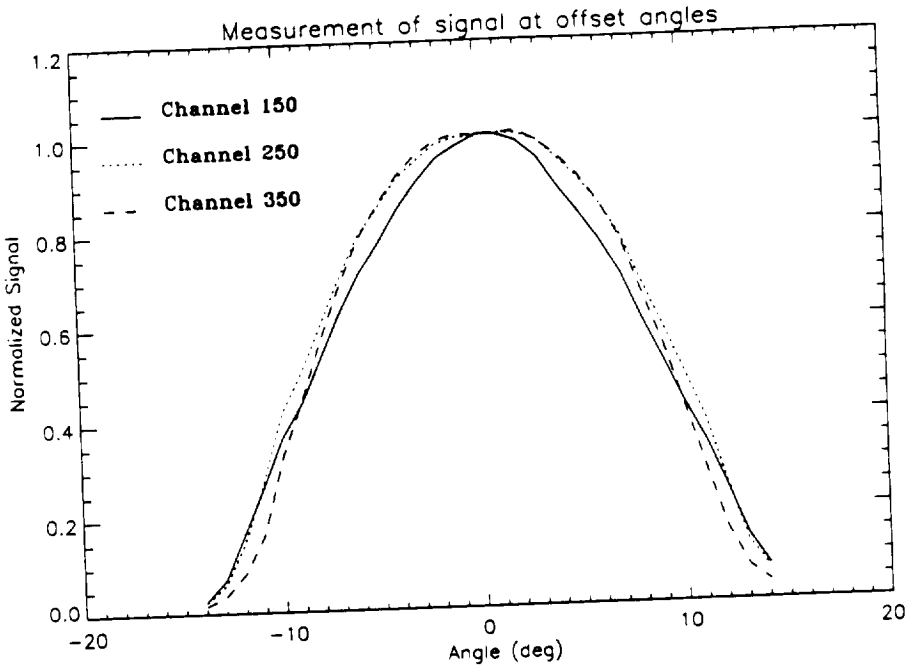

Figure D.1: Signal drop off versus off-axis viewing angle

Appendix E

Light Source

All the objects were illuminated with a 1000 Watt Quartz-Halogen light source reflected through a high precision parabolic mirror to form a highly collimated light beam which closely resembles actual solar conditions. The lamp was a commercial GE type FEL 1000-watt lamp having a tungsten coiled-coil filament enclosed in a small quartz envelope. The focal length of the Parabolic mirror was 90 inches. The resulting beam has divergences ranging between 0.5 and 0.7 degrees, based on and limited to the accuracy of the actual beam projection dimension measurements. This compares well with the actual sun conditions of 0.53 degrees. See Appendix B where Figures B.1 and B.2 show the setup of the light source.

This lamp was powered by a constant power supply source which provides a constant 8 amperes of current to the light. Figure 2.2 shows the raw data from a direct measurement of the light. This signal shows the spectrum of the light source as sensed by the spectrometer. This can be compared with the calibration of another light bulb of the same model performed by Optronic Laboratories, Inc. The spectral irradiance is given in $\frac{\text{microwatts}}{cm^2 nm}$ at a distance of 50 cm when the light is operated at 8.0 amperes. [1] The differences between Figs. 2.2 and E.1 are most likely due to spectrometer characteristics and some varaince in the signal produced by each bulb.

[1] Letter from Optronic Lab dated 19 March, 1986

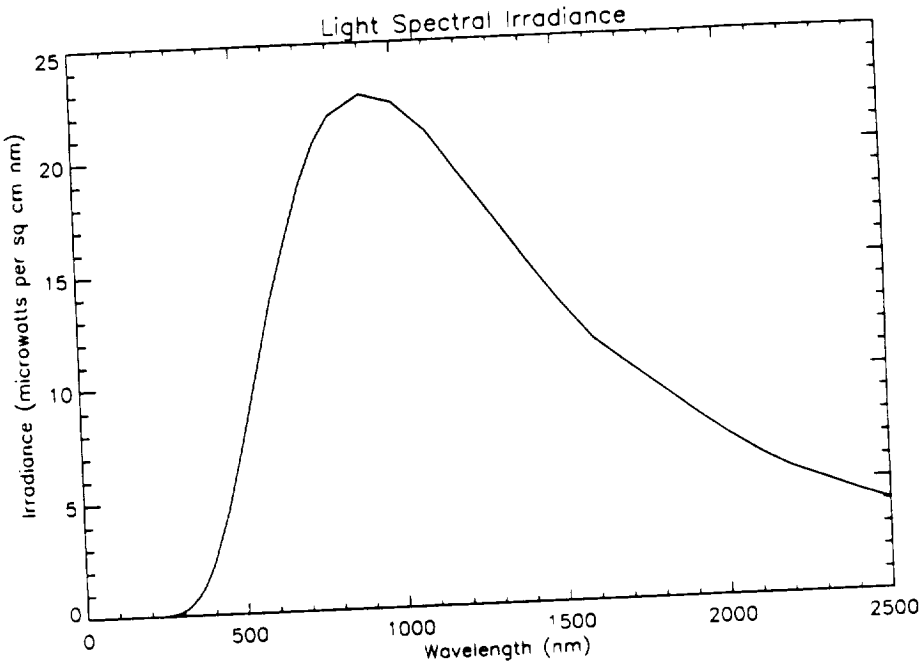

Figure E.1: Light calibration results

Appendix F

Object Handling

All tested objects were handled with equal caution. The shipping cases which contained the spheres were fastened with padlocks. At the end of each day the spheres were placed in the controlled inventory room at the Laboratory for Atmospheric and Space Physics (LASP) and secured.

Once an object was taken out of the case it was placed immediately upon the dust-free rubber ring-mount on the main mount (see Appendix B) which was surrounded by high-density foam similar to the foam inside the spheres' cases. Special lint-free gloves over latex gloves were used when handling the objects.

All of these handling procedures were rehearsed before the spheres were removed from the protective cases. As a result of the rehearsal, the experiments proceeded smoothly without incident.

Appendix G

Data Processing

This section deals with the methodology used in the data processing and handling. The following is a listing of the basic steps which were taken in analyzing the reflectance data. Several programs were written to analyze the data for each different type of object being tested. The following sections discuss the analysis of the spheres.

Data Processing Procedure

1. Take measurements.
2. Quick analysis of results.
3. Transfer data to floppy disks for more analysis and plotting.
4. Analyze the information.

G.1 Measurements

As mentioned before, the spectrometer stores information for each of is 512 channels at each phase angle. Measurements are taken at 5 degree intervals for all possible phase angles. These measurements are stored, the data is analyzed, and then the files are transferred to floppy disk for storage. This was very straightforward in the PC operating environment.

G.2 Spheres

This section discusses the data analysis for the spheres. The albedo for the spheres was calculated using two different methods. The scattering was estimated with only one method. The following paragraphs discuss some of the corrections made to the sphere data and the methods of estimating the reflectance properties.

The phase angle and range corrections discussed below come about because limitations with the setup do not allow the spheres to be viewed from a far distance. This means that the spheres do not act as a point source and will not follow the simplified reflectance equations perfectly. The corrections attempt to rectify this problem.

G.2.1 Phase angle correction

The geometry of the phase angle problem is given in Figure 2.3. Though this drawing is not to scale, it can be seen that the actual phase angle of the light off the sphere is 2ϕ instead of θ. Therefore the measured values of the phase angle are corrected to take this into account. The following equations give the relationships between the sides and angles in Figure 2.3. From the law of cosines

$$b^2 = r^2 + R^2 - 2rR\cos(\theta - \phi) \tag{G.1}$$

From the sum of angles in a triangle.

$$\gamma = 2\phi - \theta \tag{G.2}$$

From the law of sines and previous equation.

$$\theta = 2\phi - \sin^{-1}(\frac{r\sin\phi}{R}) \tag{G.3}$$

where

r	$\equiv$	Radius of sphere
R	$\equiv$	Range to sensor
b	$\equiv$	Modified range to sensor
θ	$\equiv$	Measured Phase angle
2ϕ	$\equiv$	Modified Phase angle
γ	$\equiv$	Offset angle

G.2.2 Range correction

The short range to the sensor causes other problems because the ratio $\frac{b}{R}$ is not close to 1. This means that the sphere cannot be considered a point and the distance to the reflection point changes with changing phase angle. The range from the reflecting surface to the sensor is given as b in the phase angle correction section.

There is a severe problem at this point when talking about the diffuse case. The diffuse scattering of a sphere actually would have many ranges, it is not a trivial problem. This problem is not taken into account in our formulation, but is another source of possible error. This changing range is important to take into account when fitting the data to the equation for a combination of specular and diffuse signals. The range correction is not needed for the albedo estimation which is obtained by direct integration of the reflected light.

G.2.3 Estimating albedo

The most crucial task of this experiment was to find the reflectance characteristics of the spheres so that the albedos could be found. The Albedo, sometimes referred to as the Bond Albedo (A_B), is a measure of the reflectivity of a surface, that is, the percentage of light that the surface reflects in all directions. [1] Another type of albedo is the Geometric Albedo,

[1] From Hartmann, Moons and Planets

the percentage of light reflected at zero phase angle, compared to a perfect Lambertian surface with equal projected area. [2] The Bond Albedo definition for albedo of Eqn. 4 is used in this study. The total reflected light is found by integrating the measurements over the measured phase angles, Eqns. 5-8. The total reflected light is then used to obtain the albedo estimate, Eqn. 9.

$$\text{Albedo} = \frac{\text{total reflected light}}{\text{total incident light}} \tag{G.4}$$

$$\text{Reflected Light} = \int_0^{\pi} E_r(\theta) \cdot A(\theta) d\theta \tag{G.5}$$

$$A(\theta) = \text{Area at this phase angle} \tag{G.6}$$

$$A(\theta) = 2\pi \cdot R^2(\cos\theta_1 - \cos\theta_2) \text{ for } \theta_2 > \theta_1 \tag{G.7}$$

$$A(\theta) = 4\pi \cdot R^2 \cdot \sin\theta_{ave} \cdot \sin\frac{\Delta\theta}{2} \text{ for } \Delta\theta > 0 \tag{G.8}$$

$$\text{Incident Light} = \pi r^2 \cdot E \tag{G.9}$$

These equations are implemented by numerically integrating the reflected flux over the measured phase angles. Since not all the phase angles are measured, the reflected light from the measured area is estimated. In the numerical procedure, the light intensity directed back towards the light source is assumed to be close the the values measured at small phase angles. A similar assumption is made for very large phase angles, except that the area shaded by the sphere is known not to have any reflected light. Figure G.1 shows the geometry of this problem.

G.2.4 Reflectance characteristics

The multiple phase angle measurements allow the scattering and specular signals to be decoupled for the spheres. For a perfectly specular reflection, under unobtainable ideal conditions, one would see a constant intensity from even collimated light coming off a sphere at all phase angles. For a perfectly diffuse surface one sees a very distinct falloff in signal with phase angle. Both specular and scattering characteristics are seen for the spheres in this experiment.

The surface and material properties of an object determine what type of reflectance characteristics it will have. The light reflected off an object can be thought of as either specular or scattered light. For a highly polished surface such as a mirror almost all the light reflected is specular. On the other hand, a Lambertian surface reflects (scatters) the light equally in all directions. In this experiment, it has been assumed that the spheres will reflect with a linear combination of the idealized specular and diffuse reflections.

Equations G.10 and G.11 give the ideal reflected flux of a diffuse and specular sphere viewed at a large distance. These equations come out of notes from Dr. John Lambert of Rockwell. [3]

[2] From Veverka, Planetary Satellites

[3] Personal communication with Dr. John Lambert, Rockwell Int., Colo. Spr., CO

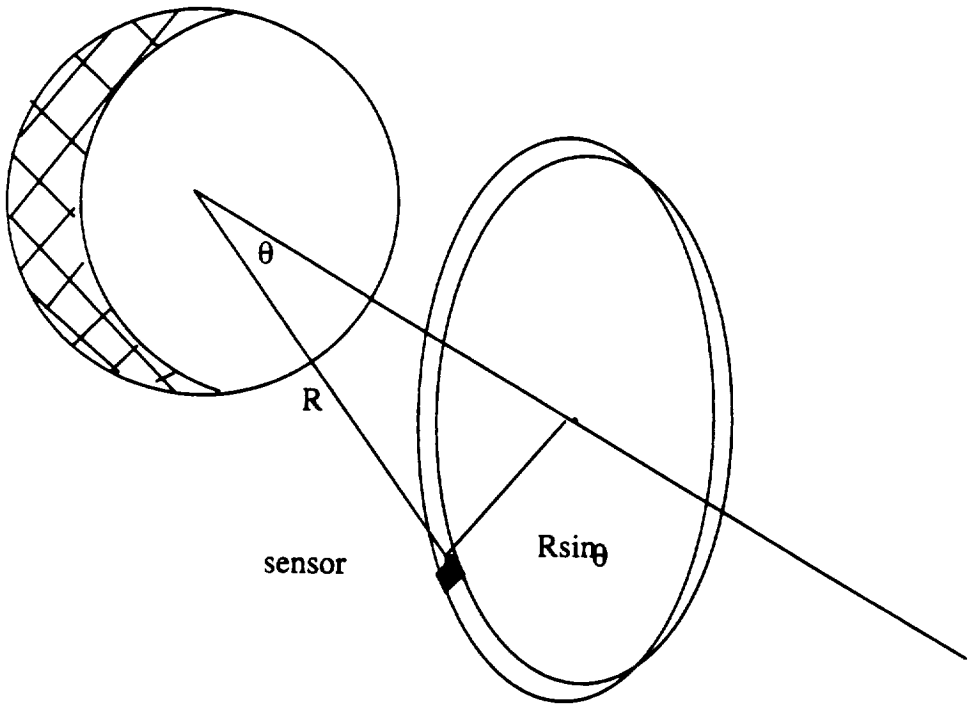

Figure G.1: Albedo calculation geometry

Diffuse sphere

$$E_r = \frac{2aEr^2}{3\pi R^2}[\sin\theta + (\pi - \theta)\cos\theta] \tag{G.10}$$

Specular sphere

$$E_r = \frac{aEr^2}{4R^2} \tag{G.11}$$

where

E_r	$\equiv$	Reflected flux
E	$\equiv$	Incident flux
a	$\equiv$	Albedo
r	$\equiv$	Radius of sphere
R	$\equiv$	Range to sensor
θ	$\equiv$	Phase angle

The equations for the specular and diffuse conditions assume that the object is either a perfect diffuse or specular object. This is not a realistic condition because to some extent

objects will have a combination of diffuse and specular reflection. Equation G.12 combines the diffuse and specular equations using the variable γ to represent the percentage of light scattered diffusely. This assumes that the reflected light can be represented by the linear combination of these two idealized signals. The term on the left hand side of the equation is referred to as the **normalized flux ratio** for the spheres. The normalized flux ratio for an idealized sphere with an albedo equal to one which scatters 50 percent of the light is shown in Fig. 2.4. This figure shows the diffuse, specular and total signals reflected.

$$\frac{E_r \cdot R^2}{E \cdot r^2} = \frac{\xi \cdot \gamma \cdot 2a}{3\pi}[\sin\theta + (\pi - \theta)\cos\theta] + (1 - \gamma) \cdot \frac{a}{4} \tag{G.12}$$

where

$$\begin{aligned} \gamma &\equiv \text{Percentage of light scattered} \\ \xi &\equiv \text{Factor for not viewing} \\ &\quad \text{the entire sphere} \end{aligned}$$

Values for the percentage of specular and diffusely reflected light may be obtained by estimating the values of γ and a in Eqn 12. This technique is able to estimate the albedo and scattering even with a limited set of data, though sometimes the fit does not follow the data trends accurately. In Eqn. 12, the reflected light signal depends non-linearly upon the phase angle and linearly on the albedo. Numerical non-linear fitting techniques are used to estimate the values for the albedo and percent of light scattered, γ. [4]

Equations G.10 - G.12 use the far field approximation – that the object is far enough away to treat it as a point source. Due to limitations within this experiment, this approximation was violated. The equation for the specular reflection off a sphere is easily modified for the close range measurements. The derivation without the far field approximation was done by modifying notes from Dr. John Lambert of Rockwell Int., Colo. Spr., CO. Figure G.2 shows the geometry for the specular case. The incoming light has an intensity E which is incident upon a small area defined as $\frac{\pi(r \cdot di)^2}{4}$. The reflected light has an intensity E_r which is even over the area $\frac{\pi(r \cdot di + 2 \cdot b \cdot di)^2}{4}$. The total reflected light equals the total incident light times the albedo. This yields:

$$\text{Specular } E_r = \frac{aEr^2}{(4b^2 + 4br + r^2)} \tag{G.13}$$

It can be seen that in the limit as b approaches zero, and for values of b much greater than r, this equation converges to the previous specular equation. This derivation is obtained by assuming area of the incoming light can be approximated by the the area given above. This derivation is not strictly correct, but should model the range correction much better than the idealized equations.

The derivation of the equations for the spheres was not integrable in the modified form. The equation can be numerically integrated for specific sphere sizes and ranges to the sensor. Due to the non-integrability of the diffuse equations, the spheres were evaluated using this range correction.

[4] Numerical Recipes

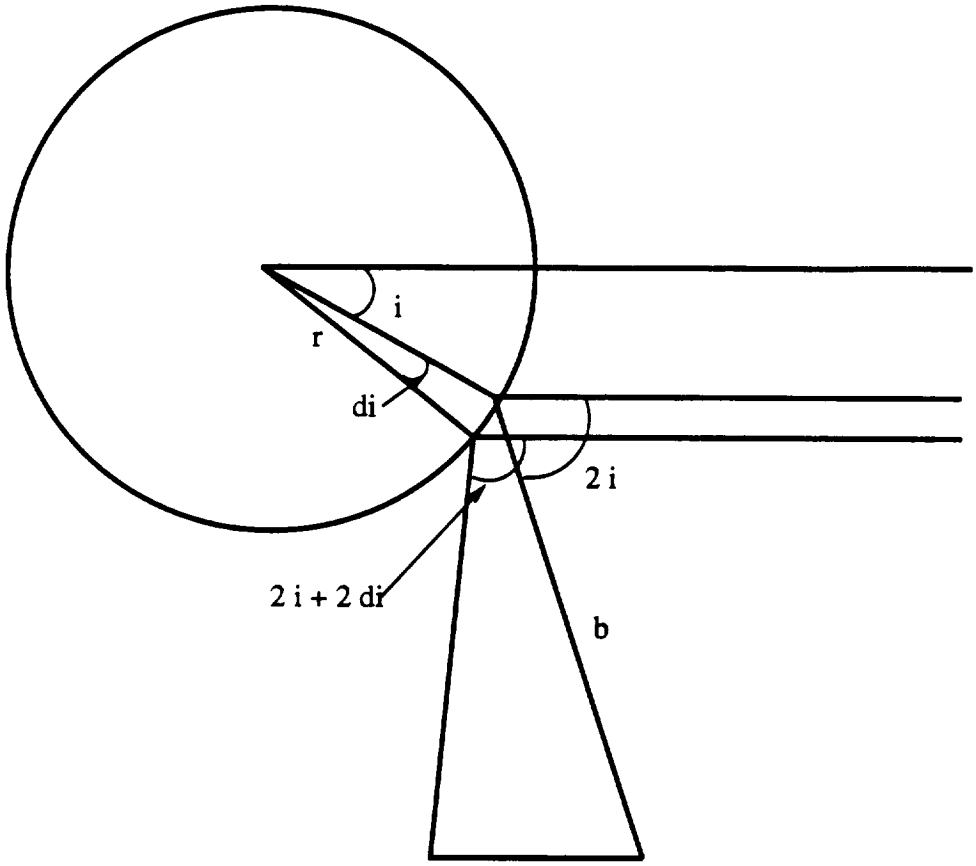

Figure G.2: Geometry for specular sphere reflection

G.2.5 Analysis and presentation of the sphere information

The information from this study is presented in both tabular and graphic format to illustrate the properties of each sphere. A PC FORTRAN program has been written to analyze the data after the measurements are taken to verify that the data looks reasonable. The basic program flow is outlined below.

Sphere albedo analysis

1. Read in the light signal.
2. Read in the measurements at different phase angles.
3. Correct for the spectrometer drift.
4. Calculate the albedo by the direct integration method.
5. Correct for the phase angle and range to sphere.
6. Calculate the albedo and scattering by non-linear parameter fit.
7. Utilize a UNIX platform for printing and plotting results.

G.3 Data organization

The data for this project was organized according to the naming convention used by Lockheed. Additional information regarding the test number was also included in the data file names. An example of the naming convention used is: SN1008T1.035, which indicates the data file in question is the 35th data file (.035) of the first test (T1) on the SN1008 white sphere.

Appendix H

Flight Sphere Results

The plots generated from the flight sphere data are presented in this appendix. Table H.1 summarizes which figures correspond to which flight sphere. Five tests were performed on each sphere. The first two figures show the albedo-scattering plots for each white sphere, while the second two figures show the best fit and raw data for each of the two spheres.

Sphere ID	Size of Sphere	Type of Sphere	Albedo	Deviation	Scattering	Deviation
SN1008	4	White	.7794	.041	.8168	.014
SN1012	4	White	.7654	.031	.8216	.054

Table H.1: Scattering and albedo values for white spheres

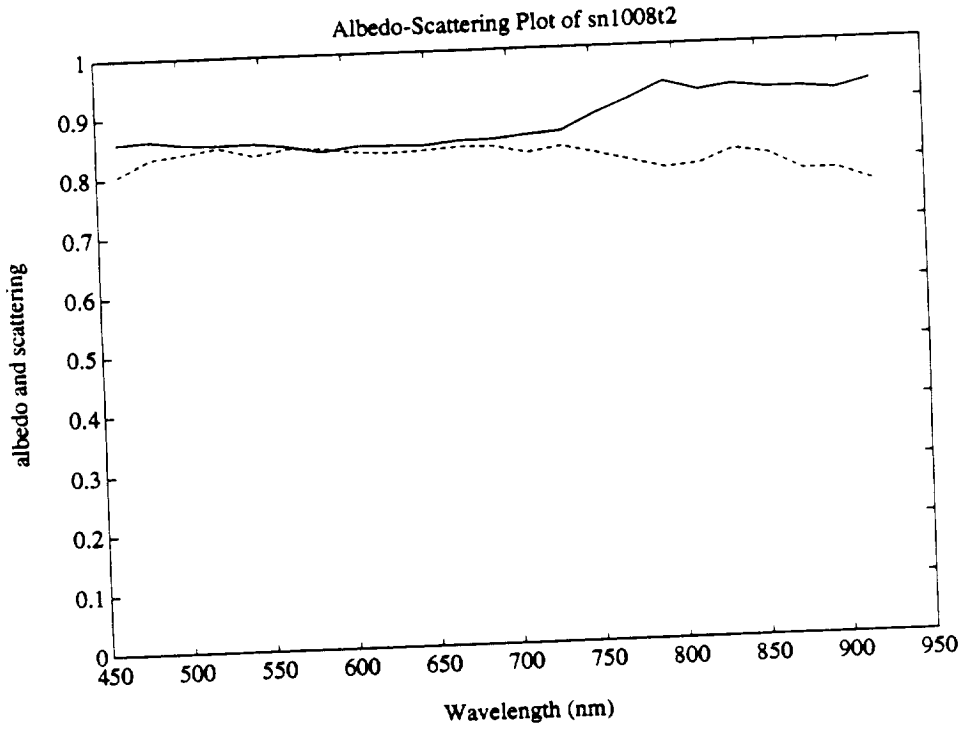

Figure H.1: 4 inch white flight sphere ID number sn1008

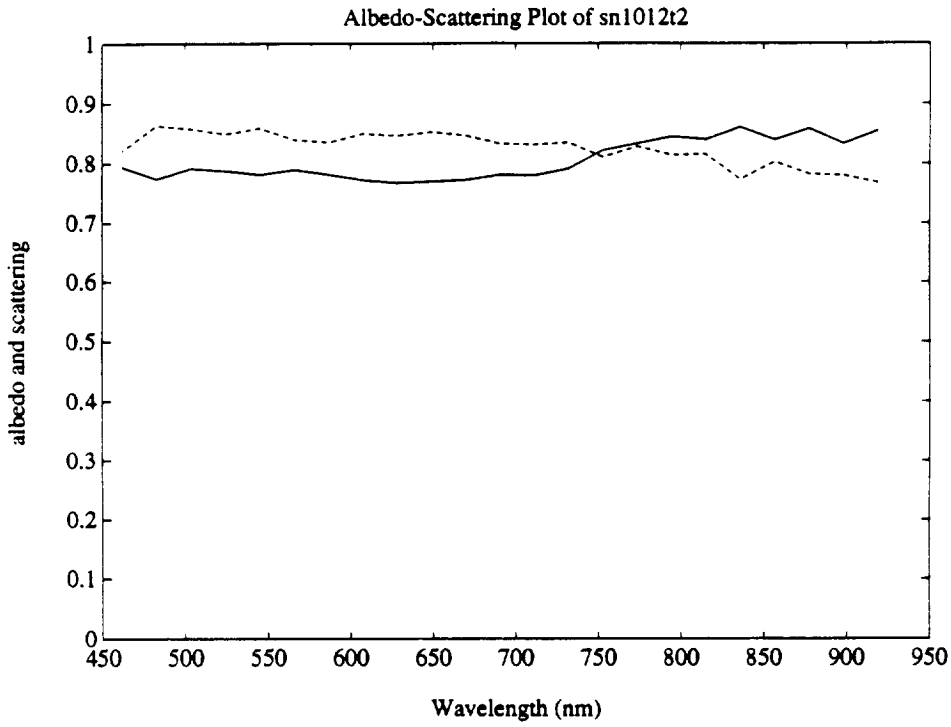

Figure H.2: 4 inch white flight sphere ID number sn1012

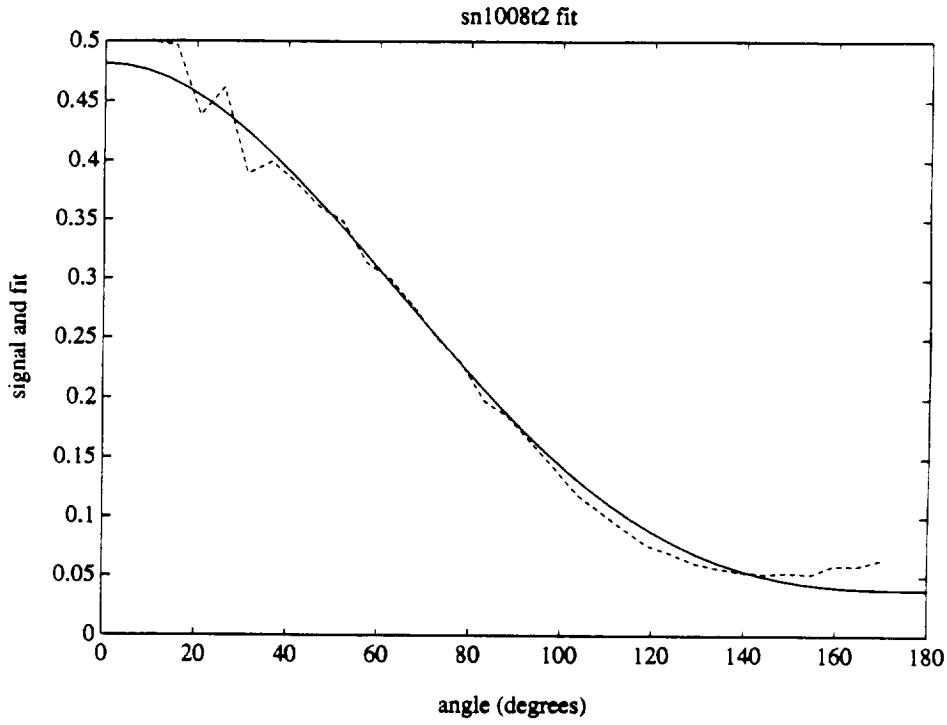

Figure H.3: 4 inch white flight sphere ID number sn1008

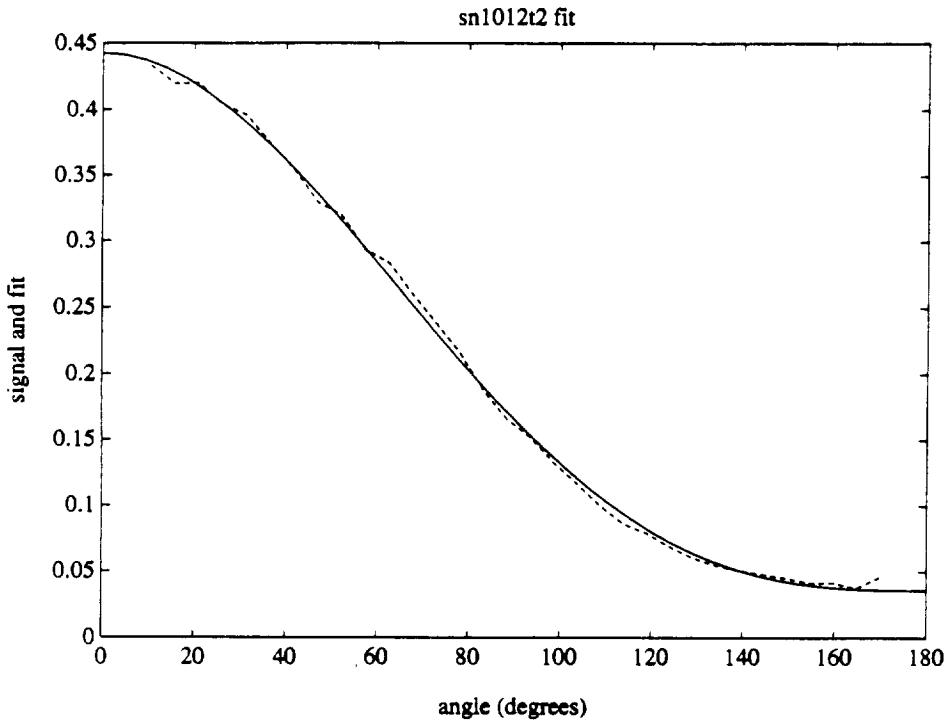

Figure H.4: 4 inch white flight sphere ID number sn1012